

See discussions, stats, and author profiles for this publication at: <https://www.researchgate.net/publication/236595211>

Application of Remote Sensing to Coastal Ecosystem Management

Conference Paper · May 2002

CITATIONS

3

READS

3,142

4 authors, including:



Victor Klemas

University of Delaware

257 PUBLICATIONS 6,029 CITATIONS

[SEE PROFILE](#)



Xiao-Hai Yan

University of Delaware

171 PUBLICATIONS 3,206 CITATIONS

[SEE PROFILE](#)

Some of the authors of this publication are also working on these related projects:



Deeper Ocean Remote Sensing [View project](#)



Hyperspectral Infrared Imager (HyspIRI) - Aquatic Study Group (ASG) [View project](#)



www.cerf-jcr.org

Remote Sensing Techniques for Studying Coastal Ecosystems: An Overview

Victor Klemas

College of Earth
Ocean and Environment
University of Delaware
Newark, DE 19716, U.S.A.
klemas@udel.edu

ABSTRACT

KLEMAS, V., 2011. Remote sensing techniques for studying coastal ecosystems: an overview. *Journal of Coastal Research*, 27(1), 2-17. West Palm Beach (Florida), ISSN 0749-0208.



Advances in sensor design and data analysis techniques are making remote sensing systems practical and attractive for use in research and management of coastal ecosystems, such as wetlands, estuaries, and coral reefs. Multispectral and hyperspectral imagers are available for mapping coastal land cover, concentrations of organic/inorganic suspended particles, and dissolved substances in coastal waters. Thermal infrared scanners can map sea surface temperatures accurately and chart coastal currents, while microwave radiometers can measure ocean salinity, soil moisture, and other hydrologic parameters. Radar imagers, scatterometers, and altimeters provide information on ocean waves, ocean winds, sea surface height, and coastal currents, which strongly influence coastal ecosystems. Using airborne light detecting and ranging systems, one can produce bathymetric maps, even in moderately turbid coastal waters. Since coastal ecosystems have high spatial complexity and temporal variability, they frequently have to be observed from both satellite and aircraft in order to obtain the required spatial, spectral, and temporal resolutions. A reliable field data collection approach using ships, buoys, and field instruments with a valid sampling scheme is required to calibrate and validate the remotely sensed information. The objective of this paper is to present an overview of practical remote sensing techniques that can be used in studies of coastal ecosystems.

ADDITIONAL INDEX WORDS: *Wetland mapping, estuaries, coral reefs, eutrophication, coastal habitat.*

INTRODUCTION

Coastal wetlands, estuaries, and coral reefs represent highly productive and critical habitats for a wide variety of plants, fish, shellfish, and other wildlife. Wetlands also provide flood protection, protection from storm and wave damage, water quality improvement through filtering of agricultural and industrial waste, and recharge of aquifers. After years of degradation due to dredge and fill operations, impoundments, urban development, subsidence/erosion, toxic pollutants, and eutrophication, wetlands and estuaries are finally receiving public attention and protection (Morris *et al.*, 2002; Odum, 1993).

In addition to immediate impacts due to anthropogenic activities, global warming and sea-level rise (SLR) will have serious long-term consequences for coastal ecosystems, such as wetlands and coral reefs. The rate of SLR around the world has increased over the past century to an average of about 3 mm a year, as a result of melting glaciers and the expansion of ocean water as it warms. The Intergovernmental Panel on Climate Change estimates that the rate of SLR will accelerate in the future, with an upper range of SLR of 0.59 m by 2100 (IPCC, 2007). Based on the observed acceleration of SLR, some scientists are estimating a SLR of more than a meter by 2100

(Church and White, 2006). This substantial SLR and more frequent storms predicted for the next 100 years will impact coastal wetlands, beach erosion control strategies, salinity of estuaries and aquifers, coastal drainage systems, and coastal economic development.

Coastal areas such as barrier islands, beaches, and wetlands are highly sensitive to sea-level changes. Rising seas will intensify coastal flooding and increase the erosion of beaches, bluffs, and wetlands, as well as threaten jetties, piers, seawalls, harbors, and waterfront property. Along barrier islands, the erosion of beachfront property by flooding water will be severe, leading to greater probability of overwash during storm surges (NOAA, 1999). Rapid SLR can cause segmentation of barrier islands or disintegration of wetlands, especially if the sediment supply cannot keep up with the SLR. Furthermore, as the ocean surface water warms, stronger storms are predicted for the coasts of the Atlantic and the Gulf of Mexico. A major hurricane can devastate a wetland. For instance, during hurricanes Katrina and Rita, several hundred square miles of Louisiana wetlands practically vanished.

With the wide variety of remote sensing systems available, choosing the proper data source for observing landcover and coastal waters can be challenging. Characteristics often used to describe and compare these analogue and digital systems are grouped into four different types of resolution: spatial, spectral, radiometric, and temporal. Spatial resolution is a measure of sharpness or fineness of spatial detail. It determines the

DOI: 10.2112/JCOASTRES-D-10-00103.1 received 13 July 2010; accepted in revision 10 August 2010.

Published Pre-print online 8 November 2010.

© Coastal Education & Research Foundation 2011



Figure 1. The MODIS on NASA's *Terra* satellite captured this image on September 26, 2008, thirteen days after Hurricane Ike came ashore. The brown areas in the image are the result of a massive storm surge that Ike pushed far inland over Texas and Louisiana causing a major marsh dieback. Credits: NASA/GSFC.

smallest object that can be resolved by the sensor, or the area on the ground represented by each picture element (pixel). For digital imagery, spatial resolution corresponds to the pixel size. Spatial resolution is often represented in terms of distance (*e.g.*, 30 m, 1 km, *etc.*) and describes the side-length of a single pixel.

Spectral resolution is a measure of the specific wavelength intervals that a sensor can record. For example, while normal color photographs show differences in the visible region of the electromagnetic spectrum, color infrared photographs and the majority of digital sensors can provide information from both visible and infrared (IR) regions of the spectrum. For digital images, spectral resolution corresponds to the number and location of spectral bands, their width, and the range of sensitivity within each band (Jensen, 2007).

Radiometric resolution is a measure of a sensor's ability to distinguish between two objects of similar reflectance. Radiometric resolution can be thought of as the sensor's ability to make fine or "subtle" distinctions between reflectance values. For example, while the *Landsat* thematic mapper (TM) has a radiometric resolution of 256 (8 bits), the moderate resolution imaging spectrometer (MODIS) has a radiometric resolution of

4,096 (12 bits). This means TM can identify 256 different levels of reflectance in each band, while MODIS can differentiate 4,096; thus MODIS imagery can potentially show more and finer distinctions between objects of similar reflectance (Campbell 2007).

Temporal resolution is a measure of how often the same area is visited by the sensor. Temporal resolution does not describe a single image, but rather a series of images that are captured by the same sensor over time. While the temporal resolution of satellite imagery depends on the satellite's orbit characteristics, aerial photography obviously requires special flight planning for each acquisition.

Most coastal ecosystems exhibit extreme variations in areal extent, spatial complexity, and temporal variability. Protecting them requires the ability to monitor their biophysical features and controlling processes at high spatial and temporal resolutions. Satellite and airborne remote sensors can now map and measure coastal ecosystems and their changes cost-effectively at appropriate scales and resolutions, minimizing the need for extensive field and ship measurements. This is illustrated in Figure 1, which shows an image of the Texas

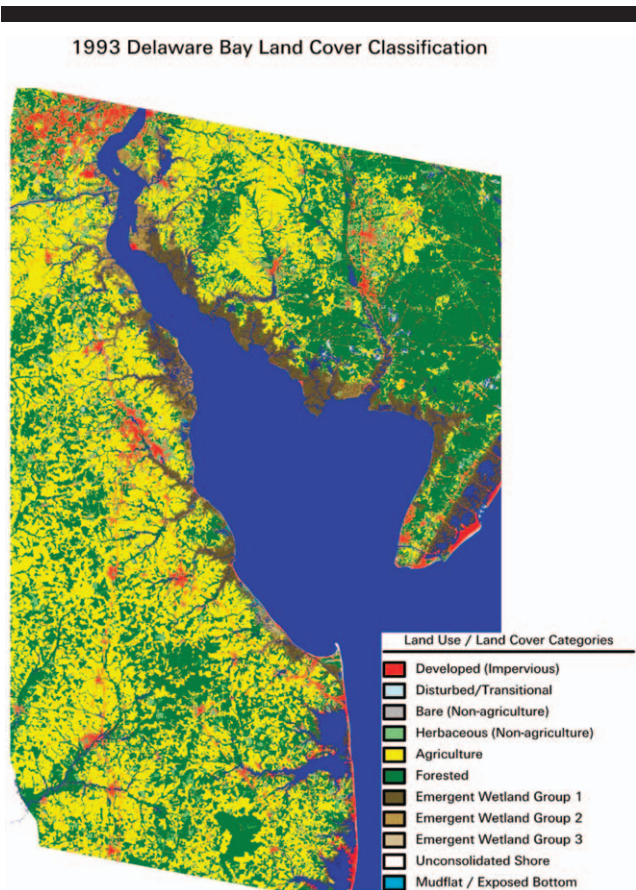


Figure 2. Delaware Bay landcover classification from 1993 based on *Landsat* TM imagery. Modified from Weatherbee (2000).

coast captured by the MODIS sensor on the National Aeronautics and Space Administration's (NASA's) *Terra* satellite 13 days after Hurricane Ike made landfall on September 13, 2008. The storm's surge covered hundreds of kilometers of the Gulf Coast because Ike was a large storm, with tropical-storm-strength winds stretching more than 400 km from the center of the storm. Most of the shoreline in this region is coastal wetland. One can clearly distinguish the brown areas in the image, which are the result of the massive storm surge that Ike had pushed far inland over Texas and Louisiana, causing a major marsh dieback. The salty water burned the plants, leaving them wilted and brown. The brown line corresponds with the location and extent of the wetlands. North of the brown line, the vegetation gradually transitions to pale green farmland and dark green natural vegetation untouched by the storm's surge. The powerful tug of water returning to the gulf also stripped marsh vegetation and soil off the land. Therefore, some of the brown seen in the wetlands may be deposited sediment. Plumes of brown water are visible as sediment-laden water drains from rivers and the coast in general. The muddy water slowly diffuses, turning pale green, green, and finally blue as it blends with clearer Gulf water (NASA/GSFC, 2010; Ramsey and Rangoonwala, 2005).

To obtain the required spatial, spectral, and temporal resolutions, coastal ecosystems frequently have to be observed

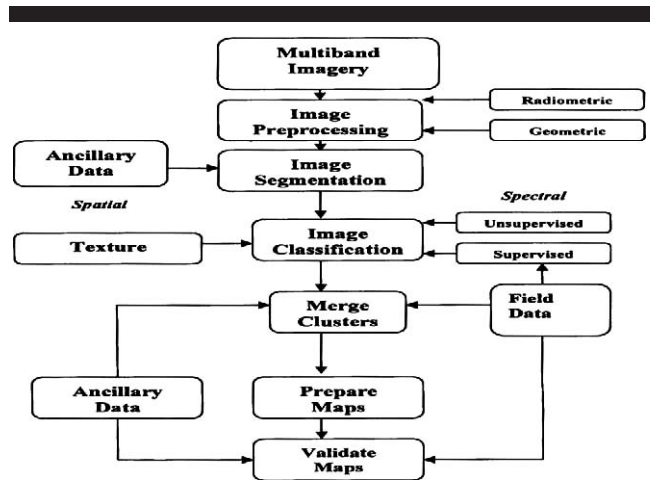


Figure 3. Typical image analysis approach.

from both satellite and aircraft. Some of the ecosystem health indicators that can be observed by remote sensors include natural vegetation cover, wetland loss and fragmentation, wetland biomass change, percentage of impervious watershed area, buffer degradation, and changes in hydrology, water turbidity, chlorophyll concentration, eutrophication level, salinity, temperature, *etc.* (Lathrop, Cole, and Showalter, 2000; Martin, 2004; Wang, 2010).

MAPPING COASTAL WETLANDS AND WATERSHEDS

To study the impact of land runoff on estuarine and coastal ecosystems, a combination of models is frequently used, including watershed models, hydrodynamic models, water quality models, and living resource models (Li *et al.*, 2007; Linker *et al.*, 1993). Most coastal watershed models require land cover or land use as an input. With input regarding how the land cover is changing, these models, together with a few other inputs like slope and precipitation, can predict the amount and type of runoff into rivers, bays, and estuaries and how these ecosystems will be affected (Jensen, 2007). The *Landsat* TM has been a reliable source for land cover data. Its 30-m resolution and spectral bands have proved adequate for observing land cover changes in large coastal watersheds (*e.g.*, Chesapeake Bay). Figure 2 shows a land cover map derived from a *Landsat* TM image, acquired in 1993, of the Delaware Bay region containing 11 landcover classes. Note that the map in Figure 2 includes three wetland, five upland, and two water classes, as required by that study (Weatherbee, 2000). Other similar satellites with medium-resolution imagers can also be used (Klemas, 2005).

A typical digital image analysis approach for classifying coastal wetlands or land cover is shown in Figure 3. Before analysis, the multispectral imagery must be radiometrically and geometrically corrected. The radiometric correction reduces the influence of haze and other atmospheric scattering particles and any sensor anomalies. The geometric correction compensates for the Earth's rotation and for variations in the position

Table 1. *High-resolution satellite parameters and spectral bands (DigitalGlobe, 2003; Orbimage, 2003; Parkinson, 2003; Space Imaging, 2003).*

Parameter	Spectral Band	<i>IKONOS</i>	<i>QuickBird</i>	<i>OrbView-3</i>	<i>WorldView-1</i>	<i>GeoEye-1</i>	<i>WorldView-2</i>
Sponsor		Space Imaging	DigitalGlobe	Orbimage	DigitalGlobe	GeoEye	DigitalGlobe
Date launched		September 1999	October 2001	June 2003	September 2007	September 2008	October 2009
Spatial resolution (m)	Panchromatic	1.0	0.61	1.0	0.5	0.41	0.5
	Multispectral	4.0	2.44	4.0	n/a	1.65	2
Spectral range (nm)	Panchromatic	525–928	450–900	450–900	400–900	450–800	450–800
	Coastal blue	n/a	n/a	n/a	n/a	n/a	400–450
	Blue	450–520	450–520	450–520	n/a	450–510	450–510
	Green	510–600	520–600	520–600	n/a	510–580	510–580
	Yellow	n/a	n/a	n/a	n/a	n/a	585–625
	Red	630–690	630–690	625–695	n/a	655–690	630–690
	Red edge	n/a	n/a	n/a	n/a	n/a	705–745
	NIR	760–850	760–890	760–900	n/a	780–920	770–1,040
Swath width (km)		11.3	16.5	8	17.6	15.2	16.4
Off nadir pointing		±26°	±30°	±45°	±45°	±30°	±45°
Revisit time (days)		2.3–3.4	1–3.5	1.5–3	1.7–3.8	2.1–8.3	1.1–2.7
Orbital altitude (km)		681	450	470	496	681	770

and attitude of the satellite. Image segmentation simplifies the analysis by first dividing the image into homogeneous patches or ecologically distinct areas. Supervised classification requires the analyst to select training samples from the data that represent the themes to be classified (Jensen, 1996). The training sites are geographic areas previously identified using field visits or other reference data, such as aerial photographs. The spectral reflectances of these training sites are then used to develop spectral “signatures,” which will be used to assign each pixel in the image to a thematic class.

Next, an unsupervised classification is performed to identify variations in the image not contained in the training sites. In unsupervised classification, the computer automatically identifies the spectral clusters representing all features on the ground. Training site spectral clusters and unsupervised spectral classes are then compared and analyzed using cluster analysis to develop an optimal set of spectral signatures. Final image classification is then performed to match the classified themes with the project requirements (Jensen, 1996). Note that throughout the process, ancillary data are used whenever available (*e.g.*, aerial photos, maps, field samples, *etc.*).

When studying wetland sites or small watersheds one can use aircraft or high-resolution satellite systems (Adam, Mutanga, and Rugege, 2010; Klemas, 2005). Airborne georeferenced digital cameras, providing color and color-IR digital imagery are particularly suitable for accurate mapping or interpreting satellite data. Most digital cameras are capable of recording reflected visible to near-IR light. A filter is placed over the lens that transmits only selected portions of the wavelength spectrum. For a single camera operation, a filter is chosen that generates natural color (blue–green–red wavelengths) or color-IR (green–red–near-IR wavelengths) imagery. For multiple camera operations, filters that transmit narrower bands are chosen. For example, a four-camera system may be configured so that each camera filter passes a band matching a specific satellite imaging band, *e.g.*, blue, green, red, and near-infrared (NIR) bands matching the bands of the *IKONOS* satellite multispectral sensor (Ellis and Dodd, 2000).

Such digital imagery can be integrated with global positioning system (GPS) position information and used as layers in a

geographic information system (GIS) for a wide range of modeling applications (Lyon and McCarthy, 1995). Small aircraft flown at low altitudes (*e.g.*, 500 m) can be used to supplement field data. High-resolution imagery (0.6 m to 4 m) can also be obtained from satellites, such as *IKONOS* and *QuickBird* (Table 1). However, cost becomes excessive if the site is larger than a few hundred square kilometers, and in that case, medium-resolution sensors, such as *Landsat TM* (30 m) and *SPOT* (20 m), become more cost-effective. Wetland species identification is difficult; however, some progress is being made using hyperspectral imagers (Jensen *et al.*, 2007; Klemas, 2009a; Porter *et al.*, 2006; Schmidt *et al.*, 2004; Yang *et al.*, 2009). Hyperspectral imagers may provide several hundred spectral bands as compared with multispectral imagers, which use less than a dozen bands.

In 2004 the National Oceanic and Atmospheric Administration’s (NOAA’s) National Estuarine Research Reserve System (NERRS) Program funded a team of remote sensing experts to compare the cost, accuracy, reliability, and user-friendliness of four remote sensing approaches for mapping land cover, emergent wetlands, and submerged aquatic vegetation. The four remote sensing systems evaluated include aerial hyperspectral (AISA), aerial multispectral (ADS 40, DMC), *IKONOS* (or *QuickBird*), and *Landsat TM*. Four NERRS test sites were selected for the project, including the ACE Basin, South Carolina; Grand Bay, Michigan; St. Jones River & Blackbird Creek, Delaware; and Padilla Bay, Washington. Completed in 2006, this study found that aerial hyperspectral image analysis is too complicated for typical NERRS site personnel, and the imagery is too expensive for large NERRS sites or entire watersheds. Owing to different sun angles for each flight strip, a separate atmospheric correction had to be implemented. Also, the aircraft roll due to wind conditions produced uneven swaths. Furthermore, it was difficult to discriminate wetlands species even with hyperspectral imagery (Porter *et al.*, 2006).

In the NERRS study, the highest accuracy for mapping clusters of different plant species over small critical areas was obtained by visually analyzing orthophotos produced by airborne digital cameras. The visual interpretation was performed after image segmentation and with the help of field

training sites visited before and after the interpretation process. For larger sites, combining *IKONOS* and *Landsat* TM proved cost-effective and user-friendly, if the *Landsat* TM imagery was used to map land cover for the large site or entire watershed and the *IKONOS* high-resolution imagery was used for detailed mapping of critical NERRS areas or those identified by *Landsat* TM as having changed. A particularly effective technique developed by the team is based on using biomass change as a habitat change indicator (Klemas, 2007; Porter *et al.*, 2006).

MONITORING WETLAND CHANGES AND LANDCOVER TRENDS

To identify long-term trends and short-term variations, such as the impact of rising sea levels and hurricanes on wetlands, one needs to analyze time series of remotely sensed imagery. The acquisition and analysis of time series of multispectral imagery is a difficult task. The imagery must be acquired under similar environmental conditions (*e.g.*, same time of year, sun angle, *etc.*) and in the same or similar spectral bands. There will be changes in both time and spectral content. One way to approach this problem is to reduce the spectral information to a single index, reducing the multispectral imagery into one single field of the index for each time step. In this way the problem is simplified to the analysis of time series of a single variable, one for each pixel of the images. The most common index used is the normalized difference vegetation index (NDVI), which is expressed as the difference between the red and NIR reflectances divided by their sum. These two spectral bands represent the most detectable spectral characteristic of green plants. This is because the red radiation is absorbed by the chlorophyll in the surface layers of the plant (palisade parenchyma) and the NIR is reflected from the inner leaf cell structure (spongy mesophyll) as it penetrates several leaf layers in a canopy. Thus the NDVI can be related to plant biomass or stress, since the NIR reflectance depends on the abundance of plant tissue and the red reflectance indicates the surface condition of the plant. It has been shown by researchers that time series of remote sensing data can be used effectively to identify long-term trends and subtle changes of NDVI by means of principal component analysis (Jensen, 2007; Young and Wang, 2000).

The preprocessing of multirate sensor imagery, when absolute comparisons between different dates are to be carried out, is much more demanding than the single-date case. It requires a sequence of operations, including calibration to radiance or at-satellite reflectance, atmospheric correction, image registration, geometric correction, mosaicking, subsetting, and masking out clouds and irrelevant features. In the preprocessing of multirate images the most critical steps are the registration of the multirate images and their radiometric rectification. To minimize errors, registration accuracies of a fraction of a pixel must be attained. The second critical requirement for change detection is attaining a common radiometric response for the quantitative analysis for one or more of the image pairs acquired on different dates. This means that variations in solar illumination, atmospheric scattering and absorption, and detector performance must be normalized,

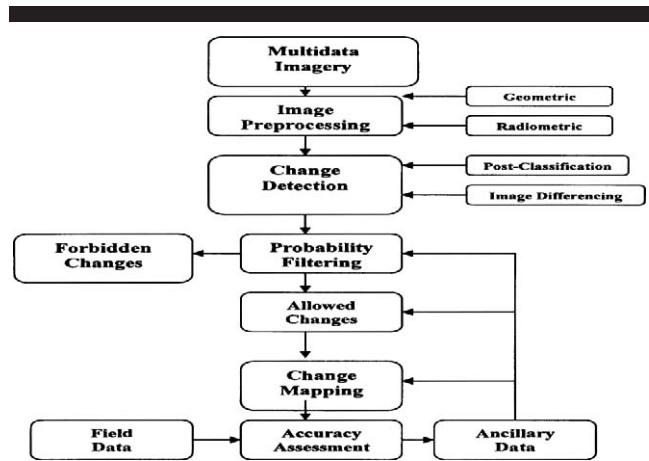


Figure 4. Change detection using probability filters.

i.e., the radiometric properties of each image must be adjusted to those of a reference image (Coppin *et al.*, 2004).

Detecting changes between two corrected images from different dates can be accomplished directly by employing one of several techniques, including postclassification comparison and temporal image differencing (Dobson *et al.*, 1995; Jensen, 1996; Lunetta and Elvidge, 1998). Postclassification comparison change detection requires rectification and classification of the remotely sensed images from both dates. These two maps are then compared on a pixel-by-pixel basis. One disadvantage is that every error in the individual date classification maps will also be present in the final change detection map.

Temporal image differencing minimizes this problem by performing the traditional classification of only one of the two time-separated images. One band from both dates of imagery is then analyzed to find differences. Pixel difference values exceeding a selected threshold are considered changed. A change/no change binary mask is overlaid onto the second date image, and only the pixels deemed to have changed are classified in the second date imagery. This method usually reduces change detection errors and provides detailed from-to change class information (Jensen, 1996). As shown in Figure 4, change analysis results can be further improved by including probability filtering, allowing only certain changes and forbidding others (*e.g.*, urban to forest). A detailed, step-by-step procedure for performing change detection was developed by the NOAA Coastal Change Analysis Program and is described in Dobson *et al.* (1995) and Klemas *et al.* (1993).

SHORELINE TOPOGRAPHY AND BATHYMETRY

Topographic and hydrographic information are basic elements in studies of nearshore geomorphology, hydrology, and sedimentary processes. In order to plan sustainable coastal development and implement effective beach erosion control and coastal ecosystem protection strategies, scientists and coastal managers need information on long-term and short-term changes taking place along the coast, including beach profiles, changes due to erosion, wetlands changes due to inundation, *etc.* (Klemas, 2009b).

Table 2. LIDAR flight parameters (DGPS = differential GPS mode; KGPS = kinematic GPS mode).

Flying height	200–500 m (400 m typical)
Vertical accuracy	±15 cm
Horizontal accuracy	DGPS = ± 3 m; KGPS = ± 1 m
Max mapping depth	60 m (clear water)
Typical kd product	4
Coastal k	0.2–0.8 ($d = 5$ –20 m)
Estuarine k	1.0–4.0 ($d = 1$ –4 m)
Sounding density	3–15 m
Sun angle	18°–25° (to minimize glare)
Scan geometry	Circular (220 m swath typical)
Sea state	Low (0–1 Beaufort scale)
Water penetration	Green LIDAR (532 nm) used
Aircraft height	IR LIDAR (1,064 nm) used

To map long-term changes of the shoreline due to beach erosion, time series of historical aerial photographs and topographic maps have been used. Aerial photographs are available dating back to the 1930s, and topographic maps exist to extend the record of shoreline change to the middle to late 1800s. Such data are held by local, state, and federal agencies, including the U.S. Geological Survey (USGS) and the U.S. Department of Agriculture Soil Conservation Service. They also have various maps, including planimetric, topographic, quadrangle, thematic, orthophoto, satellite, and digital maps (Jensen, 2007; Rasher and Weaver, 1990). Time series of high-resolution satellite images have also been used to map shoreline changes, but with accuracies of the order of 1 m.

To perform a shoreline position analysis, the shoreline can be divided into segments that are uniformly eroding or accreting. Then the change in the distance of the waterline can be measured in reference to some stable feature like a coastal highway. The instantaneous water line in the image is not a temporally representative shoreline. The high water line, also referred to as the wet/dry line, is a commonly used indicator because it is visible in most images. Other indicators include the vegetation line, bluff line, or man-made shore vestments (Boak and Turner, 2005; Thieler and Danforth, 1994). The GPS and light detecting and ranging (LIDAR) have significantly improved the techniques for shoreline position analysis and beach erosion studies (Jensen, 2007; Morton and Miller, 2005). A particularly effective approach for studying sand dynamics along coastlines includes the combined use of airborne hyperspectral data and airborne LIDAR data.

To study the bathymetry of submerged coastlines, LIDAR is normally used. In LIDAR bathymetry a laser transmitter/receiver mounted on an aircraft transmits a laser pulse that travels to the air–water interface, where a portion of this energy reflects back to the receiver. The remaining energy propagates through the water column and reflects off the sea bottom. The water depth is calculated from the time lapse between the surface return and the bottom return. Since laser energy is lost due to refraction, scattering, and absorption at the water surface, at the sea bottom, and inside the water column, these effects limit the strength of the bottom return and limit the maximum detectable depth. As shown in Table 2, the LIDAR system must have a kd factor large enough to overcome the water depth and water turbidity at the study site (k = attenuation coefficient; d = max. water depth). For

instance, if a given LIDAR system has a $kd = 4$ and the turbid water has an attenuation coefficient of $k = 1$, the system will be effective only to depths of about 4 m. Beyond that depth, one may have to use acoustic echo-sounding techniques (Brock and Sallenger, 2000).

More recently, GPSs, combined with new LIDAR techniques, made it possible to obtain more accurate topographic and bathymetric maps, including shoreline positions. LIDAR surveys can now produce a ±10 cm vertical accuracy at spatial densities greater than one elevation measurement per square meter. This is important for various coastal research applications of LIDAR, including mapping change along barrier island beaches and other sandy coasts. The ability of LIDAR to rapidly survey long, narrow strips of terrain is very valuable in this application, since beaches are elongate, highly dynamic sedimentary environments that undergo seasonal and long-term erosion or accretion and are also impacted by severe storms (Krabill *et al.*, 2000; Stockdon *et al.*, 2002).

In order to develop digital flood insurance maps and data for habitat studies and vegetation identification, in 2005 the state of Delaware contracted with USGS and NASA to produce high detail elevation data using NASA's experimental advanced airborne research LIDAR, which was specifically designed to measure submerged topography and adjacent coastal land elevations. Emergency managers have been able to use these data to develop statewide inundation maps and to incorporate these data into flood and storm surge models to create an early flood warning system (Carter and Scarborough, 2010).

The interferometric synthetic aperture radar (InSAR) technique is also a good candidate as a data source for change detection both on land and in coastal areas. It can be used jointly with GPS and altimeter data, which helps to resolve the integer ambiguity in InSAR phases. Some recent innovative applications of InSAR together with altimeter observations exist in the literature (Kim *et al.*, 2009; Lu *et al.*, 2009).

SUBMERGED AQUATIC VEGETATION AND CORAL REEFS

In many parts of the world, the health of coral reefs has been declining. Coral reefs react quickly to new stressors because they thrive in a narrow range of environmental conditions and are very sensitive to small changes in temperature, light, water quality, and hydrodynamics. The decline of reefs is closely linked to human activity, since the tropical coastlines that host them are often heavily populated. Among the documented impacts on corals are global climate change (*e.g.*, increases in sea surface temperature, sea level, CO₂ saturation, frequency and intensity of storms), shifts in water quality, and impacts due to increased loading of sediment, overfishing, contaminants, and nutrients reaching coastal environments (Philpot *et al.*, 2004; Purkis *et al.*, 2002).

Mapping submerged aquatic vegetation (SAV), coral reefs, and general bottom characteristics requires high-resolution (1–4 m) multispectral/hyperspectral imagery (Mishra *et al.*, 2006; Mumby and Edwards, 2002; Philpot *et al.*, 2004; Purkis *et al.*, 2002). Coral reef ecosystems usually exist in clear water and can be classified to show different forms of coral reef, dead coral, coral rubble, algal cover, sand, lagoons, different

Table 3. *Spaceborne ocean sensing techniques. Modified from Pinet (2009), with permission of Jones and Bartlett Learning, Sudbury, Massachusetts. www.jblearning.com (Adapted from Robinson, 1985).*

Sensor Type	Type of Measurement	Oceanographic Application
Visible and NIR radiometer and imager	Backscattered solar radiation from surface layer	Surface water turbidity; phytoplankton concentration
TIR radiometer and imager	Thermal emission from sea surface	Sea surface temperature; surface heat flux
Microwave radiometer and imager	Sea surface microwave emission	Sea surface temperature; surface heat flux; salinity; sea state; soil moisture
Radar altimeter (nadir-looking)	Return time of pulse; shape of return pulse	Ocean currents and tides; significant wave height
Radar scatterometer (side-looking radar)	Strength of return pulse from different directions	Surface wind speed and direction
SAR (high-resolution imaging radar)	Strength of return pulse from small area (Doppler shift of wave frequency with distance)	Swell patterns; internal wave patterns; oil slicks

densities of seagrasses, *etc.* SAV can grow in more turbid waters and thus is more difficult to map. Aerial hyperspectral scanners and high-resolution multispectral satellite imagers, such as *IKONOS* and *QuickBird*, have been used in the past to map SAV with accuracies of about 75%, for classes including high-density seagrass, low-density seagrass, and unvegetated bottom (Akins, Wang, and Zhou, 2010; Dierssen *et al.*, 2003; Mishra *et al.*, 2006; Wolter, Johnston, and Niemi, 2005).

Recently available hyperspectral imagers should improve the SAV and coral reef mapping results significantly (Maeder *et al.*, 2002; Porter *et al.*, 2006; Purkis, Graham, and Riegl, 2008). Major advances in using airborne hyperspectral sensors offer the spatial and spectral capability to discern the subtle spectral states of a reef that can be used as indicators of coral health. Also, environmental variables describing the boundary conditions around the reefs can be related to processes occurring on the reefs themselves (Andréfouët and Riegl, 2004). The majority of airborne hyperspectral radiometers are flexible in that they can be “tuned” to the demands of a specific project, such as mapping SAV or coral reefs (Wang, 2010).

REMOTE SENSING OF OCEAN CHLOROPHYLL AND PRODUCTIVITY

The size and complexity of coastal waters makes it difficult to monitor them with ships and buoys alone. Satellites with a wide range of sensors are proving to be cost-effective for observing large ocean and coastal areas. Some of the key ocean properties that can be mapped from satellites are shown in Table 3. As shown in the table, all electromagnetic wavelength regions are employed. For instance, ocean color, chlorophyll, and productivity can be obtained with multispectral and hyperspectral imagers operating primarily in the visible part of the spectrum. Sea surface temperatures can be mapped with

thermal infrared sensors (TIR) and ocean salinity with passive microwave radiometers.

In the open ocean, biological productivity can be estimated by measuring the chlorophyll *a* concentration. It is the primary substance determining the color of so-called Case 1 waters. As shown in Table 4, satellites with multispectral and hyperspectral imagers, such as sea-viewing wide-field-of-view sensor (SeaWiFS) and MODIS, were specifically designed to monitor ocean chlorophyll concentrations and sea temperatures on a global scale (Martin, 2004; Oliver *et al.*, 2004). With the help of calibration data from buoys and ships, these satellites have been able to map chlorophyll concentrations with acceptable accuracy.

Satellite remote sensors measure the spectral radiances at the top of the atmosphere from which (after atmospheric and other corrections) the spectral radiances emerging from the ocean surface are extracted (Bagheri, Reijkoer, and Gons, 2002). The surface radiances are converted to reflectances, providing us with the spectral signatures required for identifying chlorophyll and other water constituents (McClain *et al.*, 2006; Philpot, 2007; Schofield *et al.*, 2004). To produce valid products, such as ocean chlorophyll concentrations for estimating primary productivity, a meticulous calibration and validation approach must be used. Instrumented ships, buoys, and ocean gliders are used to calibrate and validate chlorophyll *a* and total suspended sediment maps obtained with ocean color sensors. Some typical ship or buoy measurements are shown in Table 5. In coastal and estuarine waters these data must usually be obtained very close to the satellite overpass time and be statistically representative of prevailing conditions. The water samples are normally taken from the upper half meter of the water column. Sites for calibrating remotely sensed data, such as chlorophyll *a* concentrations in coastal waters, must be located at well-known points representing the entire range of variables to be measured (Barnes *et al.*, 2003).

Table 4. *Some satellite remote sensing systems used to measure ocean color. Note that the MODIS instrument is carried aboard two platforms (Terra and Aqua). Modified from Jensen (2007). Printed and electronically reproduced by permission of Pearson Education, Inc., Upper Saddle River, New Jersey (CZCS = coastal zone color scanner; MERIS = medium-resolution imaging spectrometer; ESA = European Space Agency).*

Sensor	Agency	Satellite	Operating Dates	Spatial Resolution (m)	Number of Bands	Spectral Coverage (nm)
CZCS	NASA	<i>Nimbus-7</i>	1978–86	825	6	433–12,500
SeaWiFS	NASA	<i>OrbView-2</i>	Launch 1997	1,100	8	402–885
MODIS-Terra	NASA	<i>Terra</i>	Launch 1997	250/500/1,000	36	405–14,385
MODIS-Aqua	NASA	<i>Aqua</i>	Launch 2002	250/500/1,000	36	405–14,385
MERIS	ESA	<i>Envisat-1</i>	Launch 2002	300/1,200	15	412–1,050

Table 5. Key remote sensing related ship measurements.

Direct measurements
Temperature
Secchi depth
Attenuation coefficient
Spectral reflectance (radiance and irradiance)
Salinity
pH
Water sample analysis
Chl <i>a</i>
Total suspended sediments
Dissolved organics
Nitrogen
Phosphorus
Ship data acquisition
Water samples obtained from upper 0.5 m of water column

The open ocean is biologically quite unproductive when compared to the shallow waters of the continental shelves and coastal upwelling areas. On the continental shelves, nutrients are supplied by rivers and by wave mixing of surface and bottom water. There are also upwelling regions that owe their high productivity to the persistent upward flow of deep water, which continually charges the photic zone with nutrients. Therefore, some of the world's largest fisheries are located in upwelling areas, such as the main ones located on the west coasts of North and South America, the west coast of Africa, and off the coast of Somalia. Ocean color sensors and thermal infrared imagers have been used quite successfully to monitor these upwelling areas and estimate their productivity (Pinet, 2009).

As one approaches the coast and enters the bays and estuaries, the water becomes quite turbid and contains suspended sediment, dissolved organics, and other substances, in addition to chlorophyll. To identify each substance in this complex mixture of Case 2 waters requires hyperspectral sensors and more sophisticated algorithms than the empirical regression models used in Case 1 waters in the open ocean (Bagheri, Peters, and Yu, 2005; Cannizzaro and Carder, 2006; Ikeda and Dobson, 1995; Schofield *et al.*, 2004; Sydor, 2006). Neural network approaches have been used to map chlorophyll and suspended sediment concentrations in Delaware Bay and other estuaries (Keiner and Brown, 1999). Neural networks, however, require extensive "training" with coincident ship and satellite observations of radiance, and shipboard measurements of chlorophyll and sediment concentrations. These data are needed for adjusting the neural network parameters (*i.e.*, synaptic weights between neurons in different layers).

Using platforms such as ocean gliders, remotely operated vehicles (ROVs), and autonomous underwater vehicles (AUVs), with advanced optical and acoustic sensors, marine scientists can now perform high-resolution three-dimensional measurements of biological and physical ocean features at various depths. They can view thin layers of high biological productivity at different depths and study the response of planktonic distributions and processes to physical forcing across a wide range of temporal and spatial scales. For instance, thin layers require resolutions of centimeters, whereas previous ship measurements were performed at meter depth intervals,

completely missing these biologically active and important layers (Cowles and Donaghay, 1998; Marine Technology Reporter, 2010; Schofield *et al.*, 2004).

OBSERVING EUTROPHICATION AND HAZARDOUS ALGAL BLOOMS

High concentrations of nutrients exported from agriculture or urban sprawl in coastal watersheds, or produced by coastal upwelling, are causing algal blooms in many estuaries and coastal waters. Algal blooms are harmful in that they cause eutrophic conditions, depleting oxygen levels needed by organic life and limiting aquatic plant growth by reducing water transparency. Some species of algae contain potent toxins that, even in low concentrations, can be very detrimental to marine life. This toxicity can propagate through the food chain, posing a serious threat as the contaminated organisms are consumed by predators. Seabirds, marine mammals, and even humans are at risk of illness or death if they eat shellfish tainted with algal toxins.

Most algal blooms can be observed from satellites because of their distinct color, location, or repetitive seasonal appearance. Concentrations of chlorophyll *a* (Chl *a*) and total suspended sediments can be used as indicators of the severity of eutrophication and turbidity, respectively. Another promising approach is to detect the environmental conditions suitable for bloom development and to track the progress of a bloom as it moves in from offshore (Jernakoff *et al.*, 1996). This technique could allow prediction of when and where a coastal region would be affected by a hazardous algal bloom (HAB).

One such example is the tracking of sea surface temperature (SST) features, such as fronts, where HAB species are likely to accumulate, using advanced very high resolution radiometer (AVHRR) data (Chang *et al.*, 2002; Keifer and Anderson, 1993; Tester *et al.*, 1991). Alternatively, variations in ocean color can be used for the detection of anomalously high chlorophyll content that may indicate an impending bloom (Miller *et al.*, 2006; Stumpf, 2001). Along these lines, the NOAA Coastwatch program began in 1999 to acquire SeaWiFS imagery routinely, for the purpose of developing an accurate coastal algorithm for chlorophyll. As detailed by Tomlinson *et al.* (2004), this effort was in turn used as an early warning system for HAB occurrences off the west Florida coast. Chlorophyll anomalies identified in SeaWiFS imagery were combined with wind vector data in attempts to locate and predict the transport of the toxic dinoflagellate *Karenia brevis*. A bulletin was issued warning of HAB occurrences (Stumpf *et al.*, 2003). The advantage of SeaWiFS imagery is that it provides data with a swathwidth on the order of 1,000 km and a resolution of 1 km. Repeat coverage of an area occurs approximately every 1 to 2 days.

If broad criteria are used to compare estuarine water quality and eutrophication levels, as shown in Table 6, it is possible to get satisfactory results with sensors having fewer spectral bands and lower signal-to-noise ratios than the hyperspectral imagers needed for measuring precise concentration levels. Most riverine and estuarine plumes and some ocean-dumped waste plumes can be detected remotely due to their strong surface signatures caused by high turbidity. The drift and

Table 6. *General water quality levels.*

Level	Measurement
Water quality <i>vs.</i> Chl <i>a</i> concentration	
Oligotrophic	<8 µg/L
Mesotrophic	8–25 µg/L
Eutrophic	>25 µg/L
Water quality <i>vs.</i> total suspended sediments	
Clear	0–10 mg/L
Moderately turbid	10–50 mg/L
Highly turbid	>50 mg/L
Examples	
Delaware Bay is mesotrophic and moderately to highly turbid	
Chesapeake Bay is mesotrophic to eutrophic and moderately turbid	

dispersion of coastal plumes and ocean-dumped waste have been tracked with multispectral satellite imagery. To study the dynamics of such plumes one can use a small number of multispectral bands; however, to detect the composition and concentration of their content is difficult, even with hyperspectral images (Klemas and Philpot, 1981; Ritchie, Zimba, and Everitt, 2003; Sarabun, 1993).

SEA SURFACE TEMPERATURE

Accurate large-scale, long-term observations of SST are important to a wide range of oceanographic studies. Sea surface temperatures are necessary, for example, for estimating the source of heat at the air–sea boundary. Sea surface temperature and salinity are also important input data for estimating the steric component of the sea level, which is important for coastal studies. High-resolution satellite-derived SST measurements are ideal for investigating western boundary currents, such as the Gulf Stream and Kuroshio, which exhibit displacements on large temporal and spatial scales. Another global-scale event that appears linked to elevated SSTs is damage to coral reefs. Long time series of accurate, global SSTs are needed to monitor the health of the Earth’s coral reefs, which support a large diversity of sea life. Sea surface temperature data has also been used by the fish and wildlife communities to study habitats over many parts of the globe.

Thermal infrared sensors have been deployed for over 30 years on operational meteorological satellites to provide images of cloud top and SSTs. This was the first method of remote sensing to gain widespread acceptance by the oceanographic and meteorological communities. One reason for the early success of measuring SST is as follows. Since the TIR radiance depends on both the temperature and emissivity of the target, it is difficult to measure land surface temperatures, since the emissivity will vary as the land cover changes. On the other hand, over water the emissivity is known and nearly constant (98%), approaching the behavior of a perfect black-body radiator. Thus the TIR radiance measured over the oceans will vary primarily with the sea surface temperature (SST) and allow one to determine the SST accurately ($\pm 0.5^\circ\text{C}$) if some atmospheric corrections are included (Ikeda and Dobson, 1995; Martin, 2004).

Beginning in 1981 with the launch of the AVHRR on NOAA-7, there now exist nearly three decades of IR satellite SST observations. These contribute to multiyear global climate studies and to regional support of fisheries, ship routing, physical oceanography research, and weather forecasting. Examples of long-term studies include the changes in SST patterns associated with such interannual climate variations as the La Niña and El Niño cycles in the equatorial Pacific and Atlantic.

A particularly pertinent use of near-real-time SST data products for monitoring changing climate is the NOAA “Coral Bleaching Virtual Station Program” (Liu *et al.*, 2005). Here, both a web portal and Google Earth are used to freely disseminate information concerning the likelihood that selected coral reef sites around the world will be damaged by warmer than usual sea temperatures. The products are entirely derived from the AVHRR satellite sensors, requiring no *in situ* validation (hence use of the term “virtual”). This aspect of the program is important since many of the sites covered are so remote that routine ship or buoy monitoring is unfeasible (Purkis *et al.*, 2002).

Another important application of sea surface temperature sensing is in studies of coastal upwelling, where rising cold water brings nutrients to the surface, inducing phytoplankton and zooplankton to grow and attract large concentrations of fish. Upwelling areas, such as the one off Peru’s coast, and their condition can be observed by satellites with thermal IR imagers, such as AVHRR, or ocean color sensors, including SeaWiFS (Martin, 2004; Schofield *et al.*, 2004; Yan *et al.*, 1993). When wind patterns over the Pacific Ocean change, warm waters from the Western Pacific shift to the Eastern Pacific and the upwelling of nutrient-rich cold water off the Peruvian coast is suppressed, resulting in well-recognized El Niño conditions. Thus during an El Niño episode there is little upwelling of nutrient-rich water, causing the fish population to drop to disastrous levels.

SEA SURFACE SALINITY

Sea surface salinity (SSS) is critical for determining the global water balance, for understanding ocean currents, and for estimating evaporation rates. Also, low-salinity water is frequently indicative of fresh water sources, like rivers, feeding the ocean. Such river “plumes” can transport natural and man-made river-borne contaminants into the sea and can directly stress marine ecosystems that are adapted to higher salinity levels. Airborne microwave radiometers can measure sea surface salinity and have been used in many applications, such as determining the structure and influence of river plumes on the Great Barrier Reef, since the input of freshwater plumes from rivers is a critical consideration in the study and management of coral and seagrass ecosystems (Burrage *et al.*, 2003; Burrage, Wesson, and Miller, 2008).

In microwave radiometry, the power received by the radiometer antennae is proportional to the microwave emissivity and temperature of the ocean surface. Salts dissolve in water creating charged ions and anions. These charged particles increase the reflectivity and decrease the emissivity of the water. Thus, if the water temperature can be obtained by

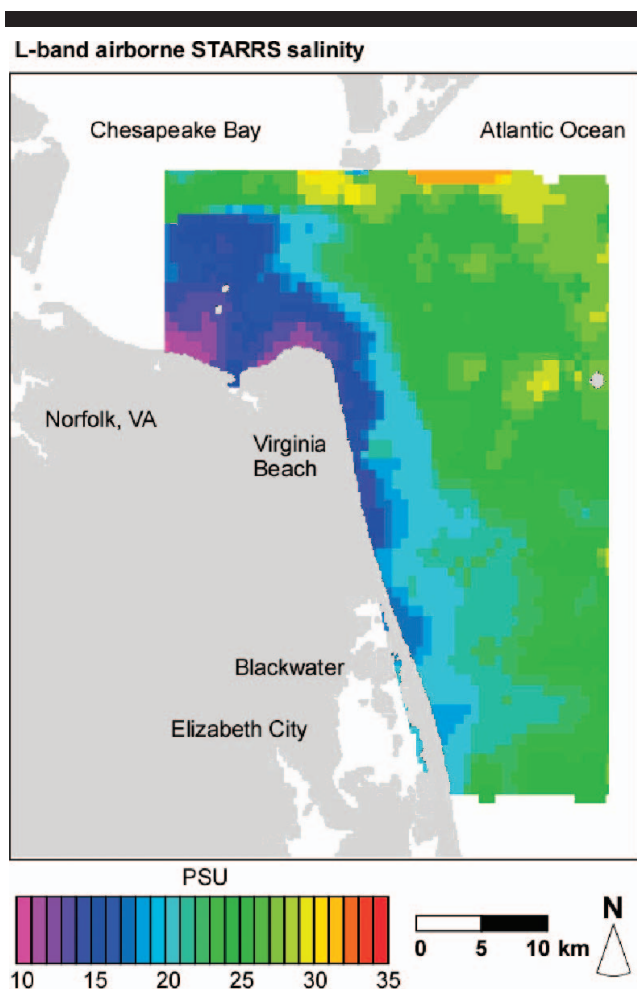


Figure 5. Sea surface salinity map of lower Chesapeake Bay produced from the salinity, temperature, and roughness remote scanner (STARRS) airborne salinity imager. The instrument is an L-band (1.4 GHz) microwave radiometer. A pronounced gradient in salinity (delivered in practical salinity units [psu]) is evident across the mouth of the bay. Modified with permission from Miller and Goodberlet (2004).

other means such as thermal IR radiometers, the salinity can be deduced from the received power. Salinity is measured in units of parts per thousand (ppt). Average seawater has a salinity of about 35 ppt. This means that the dissolved salt occurs in a concentration of 35 parts per thousand, or 3.5%, with the remaining 96.5% being water molecules. Another set of units used to measure salinity, which are related to the conductivity of the water, are practical salinity units (psu). Their numerical values are identical to ppt units. For instance, the sea surface salinity map in Figure 5, obtained with an airborne microwave radiometer, shows that the surface water salinity across the mouth of Chesapeake Bay ranges from about 12 psu to 30 psu (Miller and Goodberlet, 2004).

Sea surface salinity has been the most important oceanic variable that until recently has not been measured from satellites. There are now instruments designed to provide SSS from satellite orbit. For instance, the European *Soil Moisture and Ocean Salinity* satellite uses a fixed two-dimensional

interferometric antenna. The satellite will retrieve salinity with an accuracy of 0.1–0.2 precision salinity units (psu) at a resolution of about 50 km (Martin, 2004; Robinson, 2004).

OIL SPILL DETECTION AND TRACKING

Oil spills can destroy marine life as well as wetland and estuarine animal habitat. To limit the damage by a spill and facilitate containment and cleanup efforts, the shipping operators, oil companies, and other responsible agencies must rapidly obtain information on spill location; size and extent of the spill; direction and speed of oil movement; and wind, current, and wave information for predicting future oil drift and dispersion.

Most of the large oil spills in the oceans stem from tanker groundings, break-ups, and collisions, resulting in a large fraction of the oil spreading along the surface of the ocean and endangering marine and coastal ecosystems. They are also caused by tankers releasing their ballast water. In most of these cases a wide range of remote sensors have provided the required data for tracking and predicting the future movement of the spilled oil in a timely and reliable manner, helping guide rescue and defensive efforts, including the deployment of skimming vessels and protective booms. Users of remotely sensed data for oil spill tracking include the Coast Guard, environmental protection agencies, oil companies, shipping/insurance/fishing industries, and defense departments (Klemas, 2010).

For oil spill emergencies the main operational data requirements are fast turn-around time and frequent imaging of the site to monitor the dynamics of the spill. Remote sensors on satellites and aircraft meet these requirements by tracking the spilled oil at various resolutions and over wide areas at frequent intervals through multitemporal imaging. They also provide key inputs to drift prediction models and facilitate targeting of clean-up and control efforts. Most of these sensors use electromagnetic waves, even though acoustic sensors on boats and cameras on submerged robot-like vehicles may have to be used to view the subsurface behavior of the oil.

Table 7 summarizes the various ways of detecting oil slicks on water using electromagnetic waves. In the ultraviolet region oil fluoresces and thus appears to have a significantly higher reflectivity than water, even for very thin slicks. However, ultraviolet light is strongly scattered by the atmosphere and, in order to avoid such scattering, can be used only on aircraft at low altitudes. Ultraviolet sensors can also be confused by sun glint, wind slicks, and biogenic materials. To minimize this confusion, they are sometimes used in combination with other sensors, such as thermal IR or radar.

Visible wavelengths are used more commonly due to the availability of relatively inexpensive digital cameras on aircraft and multispectral imagers on satellites. There is also a reasonable atmospheric transmission window for visible wavelengths. In the visible region oil has a slightly higher reflectivity than water and can be even more readily detected if horizontally aligned filters are used. Oil sheen shows up as silvery and reflects light over a wide spectral region. Heavy oil appears brown, peaking in the 600 to 700 nm region, while mousse looks red-brown and peaks closer to 700 nm. Image analysts have to contend with many false signals at visible

Table 7. *Applicability of electromagnetic (EM) wave bands for oil detection.*

EM Band	Wavelength	Detection Mechanism	Contrast vs. Water	Thickness	Night Operation	Weather Limitations	False Targets
Ultraviolet	0.3–0.4 μm	Reflectivity fluorescence	Bright	No	No	Clear	Low
Visible bands	0.4–0.7 μm	Reflectivity	Bright	No	No	Clear	High
Reflected IR	0.7–3 μm	Reflectivity	Bright	No	No	Clear	High
TIR	3–14 μm	Emissivity	Dark/bright	Relative	Yes	Light fog	Medium
Radar	1–30 cm	Damped ripples	Dark	No	Yes	Heavy fog and rain	High
Passive microwave	0.2–0.8 cm	Emissivity reflectivity	Bright	Relative	Yes	Heavy fog and rain	Low

wavelengths, including sun glint, wind slicks, or biogenic material that can be mistaken for oil sheens. In some cases, sun glint can have a positive effect by enhancing the appearance of oil slicks and sheen. Improvements in sensor technology have led to the development of hyperspectral sensors, such as the airborne visible/infrared spectrometer and the airborne imaging spectrometer (AISA). A hyperspectral image consists of tens to hundreds of spectral bands and can provide a detailed spectral identification of a feature, such as differentiating between light and crude oil and detecting small concentrations of oil (Brecke and Solberg, 2005; Jensen, 2007).

At thermal IR wavelengths “optically thick” oil layers absorb solar radiation and reemit it as thermal energy in the 8 to 14 μm region. Thin oil slicks or sheen cannot be detected by thermal IR sensors. However, layers thicker than about 150 μm appear hot or bright, while layers less than about 50 μm appear cool and dark. There have been several theories proposed to explain the switch of the oil from “hot” to “cold” as the thickness of the slick decreases, but this change is not yet fully understood. This variability in apparent temperature may help distinguish thick layers of oil from thin layers, yet it also can cause interpreters to have difficulty distinguishing oil from water (Jha, Levy, and Gao, 2008).

Radar imagers such as side-looking airborne radar on aircraft and synthetic aperture radar (SAR) on satellites have the major advantage of not being bothered by cloud cover and other atmospheric effects, which frequently eliminate visible and IR wavelengths from contention (Table 7). Features found frequently in SAR data are regions of low backscatter caused by the presence of oil or other slicks on the sea surface. Synthetic aperture radar imagers view the ocean surface at incidence angles between approximately 20° and 30° from the local vertical. Capillary waves and short gravity waves cause the radar pulse to be scattered, including some backscattering to the radar transmitter. As short surface gravity waves or capillary ripples propagate through a region where an oil film is present, their energy is absorbed as the surface film strains, causing damping of these short waves. The film-covered area backscatters less energy to the radar receiver, since most of the radar pulse is reflected from the flatter surface, somewhat like light from a mirror in optics, sending the radar energy in the opposite direction, away from the radar antenna. Thus ocean surface areas covered by oil or other slicks show up as dark in radar images. For this to work, low to moderate winds must exist to create the short surface waves. Since the short waves being dampened are similar in wavelength to waves used by C- and X-band SARs, Bragg reflection can cause a strong radar return (Brecke and Solberg, 2005; Martin, 2004; Robinson, 2004).

When analyzing SAR images to distinguish oil slicks from other surface films, such as organic films generated by natural biological processes or wind-generated slicks, one must consider additional information. This can include the general shape of the slick, its proximity to oil tanker routes or oil drilling platforms, the local wind speed, and other dynamic causes, such as internal waves and ocean fronts. Large ocean internal waves on continental shelves strongly influence acoustic wave propagation; submarine navigation; mixing nutrients to euphotic zone; sediment resuspension; cross-shore pollutant transport; and coastal engineering and oil exploration. The water column is frequently not homogeneous, but stratified. Internal waves move along pycnoclines, which are surfaces that separate water masses of different densities. The larger internal waves can attain heights in excess of 20 m. The period of the internal wave packets approximates the period of the tides, suggesting a cause-and-effect relationship. Internal waves can be detected visually and by radar, since they cause local currents that modulate surface wavelets and slicks, which can be detected by radar (Zhao *et al.*, 2004).

Oil on top of the ocean is a stronger emitter of microwave radiation than water and therefore appears as a bright feature on a darker sea. The emissivity of oil is about 80%, while that of water is only about 40%. Therefore a passive microwave radiometer can detect the difference in emissivity and map the oil slicks. However, this technique has not been used much, because the signal-to-noise ratio is poor, the signal strength varies with oil layer thickness in a cyclical fashion, and other surface materials can cause false alarms (Brecke and Solberg, 2005).

Past applications indicate that radar and multispectral (visible/near-IR) scanners are most effective for detecting and tracking oil slicks over large ocean or coastal areas. Agencies like the Coast Guard perform their more detailed aerial surveillance using integrated multisensor systems, including X-band side-looking radars, IR/ultraviolet line scanners, active gated television, and aerial reconnaissance cameras. At medium altitudes these side-looking radars provide ship and oil spill detection and mapping out to 80 miles on both sides of the aircraft. The real-time television cameras provide day/night high-resolution real-time detection and identification. The reconnaissance cameras provide high-resolution daytime documentation.

REMOTE SENSING OF PHYSICAL OFFSHORE PROCESSES

Currents and waves strongly affect coastal ecosystems, especially in the nearshore, which is an extremely dynamic

environment. Currents influence the drift and dispersion of various pollutants, and together with breaking waves mobilize and transport sediments, resulting in erosion and morphological evolution of natural beaches. On a coastal scale, predicting the motion of a patch of water containing a toxic red tide algal bloom or industrial waste is vital for planning appropriate reactive measures. To predict the local movement of pollutants, one must track the currents in the area. Current meters are not effective for determining surface currents over large coastal regions, since current meters measure currents only at a point. On the other hand, radar sensors on satellites can measure sea surface currents over large areas and monitor the dynamic behavior of ocean and coastal waters.

Hydrodynamic models are commonly used to study the physical forces, such as currents, winds, and waves, acting on coastal and estuarine ecosystems. Hydrodynamic models require physical data on river flow, tides, winds, current patterns, waves, *etc.* Many of these data can be obtained using remote sensors on satellites and aircraft, with calibration and validation performed by a relatively small number of field or ship measurements (Robinson, 2004). As shown in Table 3, physical ocean properties can be measured with various radar instruments, such as winds with scatterometers, sea surface elevation and currents with altimeters, and sea surface slicks and waves with SAR. These measurements are used by oceanographers to study the ocean and coastal circulation, its large-scale, low-frequency variability, biological mixing, turbulent eddy energy, and air–sea interaction (Martin, 2004; Robinson, 2004). There are also some indirect space geodetic techniques like *Gravity Recovery and Climate Experiment (GRACE)* and *Gravity Field and Steady-State Ocean Circulation Explorer (GOCE)* missions, which provide valuable information on ocean currents globally and regionally, as well as the variations in the ocean mass and its redistribution.

Radar altimeters, scatterometers, and SAR imagers are of particular value because they provide real-time accurate information on ocean elevation, currents, winds, and waves. The application of these radars depends on the character of the pulse emitted and on what properties of the reflected pulse are measured. Satellite altimetry produces unique global measurements of instantaneous sea surface heights relative to a reference surface and is one of the essential tools for monitoring ocean surface conditions, including sea level, tidal circulation, and ocean currents. For the nadir-pointing altimeter the timing of the returned pulse after reflection from the ocean surface, knowing the speed of light (electromagnetic waves), allows one to measure the distance between the radar and the sea surface. From the altimeter-measured range, the instantaneous sea surface relative to a reference surface, such as an ellipsoid, can be determined if the satellite orbit relative to the reference surface is known. With the knowledge of the oceanic geoid, the sea surface topography relative to the geoid due to ocean dynamic circulation, including the temporal averages, can be mapped. Repeated observations can provide a measurement of the temporal variability of the sea surface height, since the geoid can be treated as time-invariant for oceanographic applications. Even though this is true, at present one can compute the geoid with a temporal resolution of 1 month using only gravity dedicated satellites like *GRACE* and *GOCE*

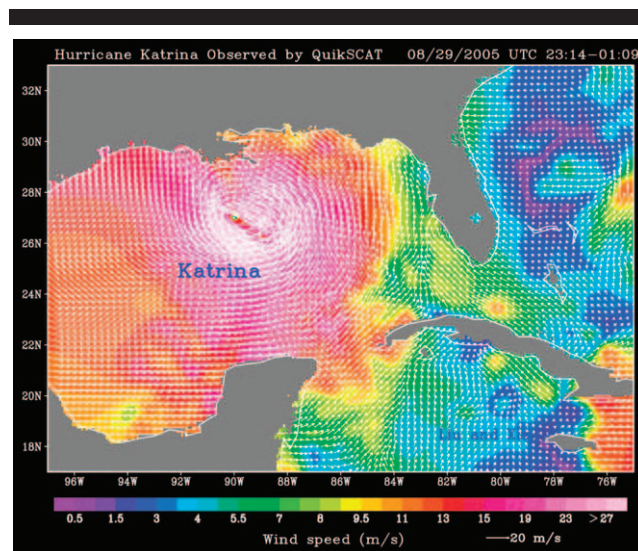


Figure 6. Hurricane Katrina generated surface winds observed by the QuickSCAT scatterometer. The arrows indicate the direction of the surface wind while the colors show the speed. Courtesy: W. Timothy Liu and Xiaosu Xie, NASA/JPL.

(Elachi and van Ziel, 2006; Ikeda and Dobson, 1995; Robinson, 2004).

For monitoring SLR along a specific coast or wetland, tide gauge stations provide useful information. If continuous GPS receivers are collocated at these stations, these data can be useful for linking the observed sea level to a vertical datum and also distinguishing the continental uplift/subsidence from the SLR.

Oblique-viewing radar instruments, which measure the backscatter from the sea surface, can be divided into two types. Those that measure average backscatter from a wide field-of-view are called scatterometers and are used primarily to measure wind characteristics, which create the surface roughness. Winds transfer energy to the surface layer of the sea, causing ripples. The ripples can develop into wavelets and waves in proportion to the magnitude and direction of the winds. Satellites equipped with radar scatterometers use the sea state to estimate the near-surface wind speed and direction (Figure 6). Thus a scatterometer is a sensor that measures the return reflection or scattering of microwave (radar) pulses sent at an oblique angle to the ocean surface from a satellite. A rough ocean surface reflects back (backscatters) to the antenna on the satellite a stronger signal than a smooth ocean surface because energy from the radar signal is reflected back more effectively when steeper waves are present than when the ocean surface is relatively smooth.

Radars that have a much finer spatial resolution, called imaging radars, such as SAR, provide maps of sea surface roughness capable of defining a variety of small and mesoscale ocean characteristics, such as wave fields, and can also track the actual oil slicks. High-resolution (10 m) SAR instruments can reveal detailed patterns of ocean waves, including wavelength (spectrum) and direction. The reason waves and swells are visible in SAR images is that the capillary waves

associated with Bragg scatter form preferentially on and just ahead of the wave crests, in part because of the curvature and in part because the troughs are sheltered from the winds while the crests are exposed. This variation in capillary wave amplitude creates the observed bright/dark pattern delineating wave fields on SAR images (Martin, 2004). Since these are active microwave systems, they penetrate clouds and function in all weather. Synthetic aperture radar is carried by satellites in low Earth orbits pointing in a direction that is at 90° to the direction of travel with its axis tilted between 15° and 60° from the local vertical (Elachi and van Ziel, 2006; Ikeda and Dobson, 1995; Robinson, 2004).

Closer to the coast, shore-based high-frequency (HF) and microwave Doppler radar systems can be used to map currents and determine swell-wave parameters over large areas with considerable accuracy (Bathgate, Heron, and Prytz, 2006; Graber *et al.*, 1997; Paduan and Graber, 1997; Teague, Vesecky, and Fernandez, 1997). The surface current measurements use the concept of Bragg scattering from a slightly rough sea surface, modulated by Doppler velocities of the surface currents. High-frequency radars can determine coastal currents and wave conditions over a range of up to 200 km (Cracknell and Hayes, 2007). For instance, Coastal Ocean Dynamics Application Radar (CODAR) is becoming an integral component of integrated ocean observing systems and is already being used to measure real-time currents in support of search and rescue operations and various scientific studies (Kohut *et al.*, 2008). While HF radars provide accurate maps of surface currents and wave information for large coastal areas, their spatial resolution, which is about 1 km, is more suitable for measuring mesoscale features than small scale currents. On the other hand, microwave X-band and S-band radars have resolutions of the order of 10 m yet have a range of only a few kilometers.

Estimates of currents over large areas, such as the continental shelves, can also be obtained by tracking the movement of Lagrangian drifters or natural surface features, which differ detectably in color or temperature from the background waters. Examples of such tracked natural features include chlorophyll plumes, patches of different water temperature, and surface slicks (Breaker *et al.*, 1994). One can also use ocean drifters, which can be specifically designed to track the movement of water (currents) at various depths. A typical design of typical Lagrangian drifters includes a float or surface buoy connected by cable to a current drogue (Klemas and Philpot, 1981). The surface float provides buoyancy, contains the electronics, and transmits data to satellites. The satellites determine the drifter's position and relay the data to ground stations. The drogue, set for a specific depth, acts like an underwater sail as it is pushed by the ocean current. Ocean drifters may also contain various instruments to measure water temperatures and a variety of other parameters. Ships and aircraft can drop these durable drifter buoys into the sea, where they normally have a survival rate of several hundred days (Davis, 1985).

As shown in Table 5, ships and buoys can provide valuable data, including water samples from various depths for chemical analysis to obtain the concentrations of chlorophyll, suspended sediments, dissolved organics, oil, and local meteorological

information. For measuring oceanographic properties and concentrations over greater depths, such as the oil distribution after the Deepwater Horizon accident in the Gulf of Mexico, there is a wide range of remotely controlled robot vehicles available, which can provide vertical profiles of ocean temperature, salinity and other data. These ROVs, AUVs, and ocean gliders can carry various instruments, including visible cameras and acoustic sensors, such as side-scan sonar for observing subsurface features, such as oil plumes (Schofield, Kohut, and Glenn, 2008).

SUMMARY AND CONCLUSIONS

Advances in technology and decreases in cost are making remote sensing and geographic information systems practical and attractive for use in coastal ecosystem studies and management. They are also allowing researchers and managers to take a broader view of ecological patterns and processes. Environmental indicators that can be detected by remote sensors are available to provide quantitative estimates of coastal and estuarine habitat conditions and trends. Such indicators include percentage of impervious watershed area, natural vegetation cover, buffer degradation, wetland loss and fragmentation, wetland biomass change, invasive species, water turbidity, chlorophyll concentration, eutrophication, *etc.* Advances in the application of GIS and various models, help to combine remotely sensed images with other georeferenced data layers, such as digital elevation models, thus providing a convenient means for modeling ecosystem behavior. A good example is the predictive modeling of the impact of SLR on coastal wetlands.

New satellites, carrying sensors with fine spatial (1–4 m) and spectral (200 narrow bands) resolutions are providing the means for more accurately detecting changes in coastal ecosystem health, including biological productivity and habitat quality. Thermal IR imagers and new satellite microwave radiometers are able to map sea surface temperatures, salinity, and soil moisture. Radar scatterometers, altimeters, and imagers (SAR) are providing more accurate information on sea surface winds, elevation, currents, wave fields and oil slicks, which can now be used in models to predict storm impact on coastal ecosystems and oil spill drift and dispersion. There are various international observing systems and databases, such as the Global Geodetic Observing System and the Global Earth Observing System of Systems, which aim to gather/archive and release all the available data sets for monitoring regional and global environmental processes and make the data available for environmental research, hazard mitigation, *etc.* At the same time, advanced software is being developed for analyzing satellite data and using it in models more effectively.

Ocean platforms, such as ocean gliders, ROVs, AUVs, and optical and acoustic sensors are now available for performing high-resolution three-dimensional measurements of biological and physical ocean features, including thin layers of high biological productivity or submerged oil plumes emanating from deepwater oil spills at various ocean depths. When these new techniques for generating, organizing, storing, and analyzing spatial information are combined with watershed, hydrodynamic, water quality, and living resource models,

coastal managers and scientists will have better means for assessing the impacts of alternative management practices on coastal ecosystems and taking corrective action early, when it is most effective.

ACKNOWLEDGMENTS

This research was in part supported by NOAA Sea Grant (NA09OAR4170070-R/ETE-15) and by the NASA-EPSCoR Program at the University of Delaware.

LITERATURE CITED

- Adam, E.; Mutanga, O., and Rugege, D., 2010. Multispectral and hyperspectral remote sensing for identification and mapping of wetland vegetation: a review. *Wetlands Ecology and Management*, 18, 281–296.
- Akins, E.R.; Wang, Y., and Zhou, Y., 2010. EO-1 Advanced Land Imager data in submerged aquatic vegetation mapping. In: Wang, Y. (ed.), *Remote Sensing of Coastal Environments*. New York: CRC Press, pp. 297–312.
- Andréfouët, S. and Riegl, B.M., 2004. Remote sensing: a key tool for interdisciplinary assessment of coral reef processes. *Coral Reefs*, 23, 1–4.
- Bagheri, S.; Peters, S., and Yu, T., 2005. Retrieval of water quality constituents concentrations from AVIRIS data in Hudson/Raritan Estuary. *International Journal of Remote Sensing*, 26, 4013–4027.
- Bagheri, S.M.; Reijkober, S., and Gons, H., 2002. Inherent and apparent optical measurements in the Hudson/Raritan estuary.” *Aquatic Ecology*, 36, 559–562.
- Barnes, R.A.; Clark, D.K.; Esaias, W.E.; Fargion, G.S.; Feldman, G.C., and McClain, C.R., 2003. Development of a consistent multi-sensor global ocean color time series. *International Journal of Remote Sensing*, 24, 4047–4064.
- Bathgate, J.; Heron, M., and Prytz, A., 2006. A method of swell parameter extraction from HF ocean surface radar spectra. *IEEE Journal of Oceanic Engineering*, 31, 812–818.
- Boak, E.H. and Turner, I.L., 2005. Shoreline definition and detection: a review. *Journal of Coastal Research*, 21, 688–703.
- Breaker, L.C.; Krasnopolsky, V.M.; Rao, D.B., and Yan, X.-H., 1994. The feasibility of estimating ocean surface currents on an operational basis using satellite feature tracking methods. *Bulletin of the American Meteorological Society*, 75, 2085–2090.
- Brecke, C. and Solberg, A.H.S., 2005. Oil spill detection by satellite remote sensing. *Remote Sensing of Environment*, 95, 1–13.
- Brock, J. and Sallenger, A., 2000. *Airborne topographic Lidar mapping for coastal science*. U.S. Geological Survey Open-File Report 01-46.
- Burrage, D.M.; Heron, M.L.; Hacker, J.M.; Miller, J.L.; Stieglitz, T.C.; Steinberg, C.R., and Prytz, A., 2003. Structure and influence of tropical river plumes in the Great Barrier Reef: application and performance of an airborne sea surface salinity mapping system. *Remote Sensing of Environment*, 85, 204–220.
- Burrage, D.; Wesson, J., and Miller, J., 2008. Deriving sea surface salinity and density variations from satellite and aircraft microwave radiometer measurements: application to coastal plumes using STARRS. *IEEE Transactions on Geoscience and Remote Sensing*, 46, 765–775.
- Campbell, J.B., 2007. *Introduction to Remote Sensing*. New York: The Guilford Press.
- Cannizzaro, J.P. and Carder, K.L., 2006. Estimating chlorophyll-a concentrations from remote-sensing reflectance in optically shallow waters. *Remote Sensing of Environment*, 101, 13–24.
- Carter, R. and Scarborough, R., 2010. Sharing Delaware’s lidar lessons. NOAA Coastal Services Center Report: *Local Strategies for Addressing Climate Change*, 2, 16–17.
- Chang, G.C.; Dickey, T.D.; Schofield, O.M.; Weidemann, A.D.; Boss, E.; Pegau, W.S.; Moline, M.A., and Glenn, S.M., 2002. Nearshore physical processes and bio-optical properties in the New York Bight. *Journal of Geophysical Research*, 107, 3133–3140.
- Church, J.A. and White, N.J., 2006. A 20th century acceleration of global sea-level rise. *Geophysical Research Letters*, 33, L01602.
- Coppin, P.; Jonckheere, I.; Nackaerts, K.; Mays, B., and Lambin, E., 2004. Digital change detection methods in ecosystem monitoring: a review. *International Journal of Remote Sensing*, 25, 1565–1596.
- Cowles, T. and Donaghay, P., 1998. Thin layers: observations of small-scale patterns and processes in the upper ocean (Editorial). *Oceanography*, 11, 1.
- Cracknell, A.P. and Hayes, L., 2007. *Introduction to Remote Sensing*. New York: CRC Press.
- Davis, R.E., 1985. Drifter observations of coastal surface currents during CODE: the method and descriptive view. *Journal of Geophysical Research*, 90, 1561–1755.
- Dierssen, H.M.; Zimmermann, R.C.; Leathers, R.A.; Downes, V., and Davis, C.O., 2003. Ocean color remote sensing of seagrass and bathymetry in the Bahamas banks by high resolution airborne imagery. *Limnology and Oceanography*, 48, 444–455.
- Digital Globe, 2003. *Quickbird Imagery Products and Product Guide* (revision 4). Boulder, Colorado: Digital Globe, Inc.
- Dobson, J.E.; Bright, E.A.; Ferguson, R.L.; Field, D.W.; Wood, L.L.; Haddad, K.D.; Iredale, III, H.; Jensen, J.R.; Klemas, V.; Orth, R.J., and Thomas, J.P., 1995. NOAA Coastal Change Analysis Program (C-CAP): Guidance for Regional Implementation. NOAA Technical Report NMFS-123. Washington, DC: U.S. Department of Commerce, 92p.
- Elachi, C. and van Ziel, Z., 2006. *Introduction to the Physics and Techniques of Remote Sensing*, 2nd edition. Hoboken, New Jersey: John Wiley and Sons.
- Ellis, J.M. and Dodd, H.S., 2000. Applications and lessons learned with airborne multispectral imaging. In: *Fourteenth International Conference on Applied Geologic Remote Sensing* (Las Vegas, Nevada).
- Graber, H.; Haus, B.; Chapman, R., and Shay, L., 1997. HF radar comparisons with moored estimates of current speed and direction: expected differences and implications. *Journal of Geophysical Research*, 102, 18749–18766.
- Ikedo, M. and Dobson, F.W., 1995. *Oceanographic Applications of Remote Sensing*. New York: CRC Press.
- IPCC (Intergovernmental Panel on Climate Changes), 2007. *Climate Change 2007: The Physical Science Basis*. Paris: WMO/UNEP. www.ipcc.ch (accessed September 9, 2010).
- Jensen, J.R., 1996. *Introductory Digital Image Processing: A Remote Sensing Perspective*, 2nd edition. Upper Saddle River, New Jersey: Prentice-Hall.
- Jensen, J.R., 2007. *Remote Sensing of the Environment: An Earth Resource Perspective*. Upper Saddle River, New Jersey: Prentice Hall.
- Jensen, R.R.; Mausel, P.; Dias, N.; Gonser, R.; Yang, C.; Everitt, J., and Fletcher, R., 2007. Spectral analysis of coastal vegetation and land cover using AISA+ hyperspectral data. *Geocarto International*, 22, 17–28.
- Jernakoff, P.; Hick, P.; Ong, C.; Hosja, W., and Grigo, S., 1996. Mapping algal blooms using airborne multispectral video and the importance of bloom dynamics in the collection of in-water data. *Marine Technology Society Journal*, 30, 36–45.
- Jha, M.N.; Levy, J., and Gao, Y., 2008. Advances in remote sensing of oil spill disaster management: state-of-the-art sensor technology for oil spill surveillance. *Sensors*, 8, 236–255.
- Keafer, B.A. and Anderson, D.M., 1993. Use of remotely-sensed sea surface temperatures in studies of *Alexandrium tamarense* bloom dynamics, in toxic phytoplankton in the sea. In: Smayda, T.M. and Shimizu, Y. (eds.), *Proceedings of the 5th International Conference on Toxic Marine Phytoplankton* (UN/FAO), Amsterdam: Elsevier. pp. 763–768.
- Keiner, L.E. and Brown, C.W., 1999. Estimating oceanic chlorophyll concentrations with neural networks. *International Journal of Remote Sensing*, 20, 189–194.
- Kim, J.W.; Lu, Z.; Lee, H.; Shum, C.K.; Swarzenski, C.M.; Doyle, T.W., and Baek, S.-H., 2009. Integrated analysis of PALSAR/Radarsat-1 InSAR and ENVISAT altimeter data for mapping of absolute water level changes in Louisiana wetlands. *Remote Sensing of Environment*, 113, 2356–2365.

- Klemas, V., 2005. Remote sensing: wetlands classification. In: Schwartz, M.L. (ed.), *Encyclopedia of Coastal Science*. Dordrecht, the Netherlands: Springer, pp. 804–807.
- Klemas, V., 2007. Remote sensing of coastal wetlands and estuaries. *Proceedings of Coastal Zone 07*. Charleston, South Carolina: NOAA Coastal Services Center.
- Klemas, V., 2009a. Sensors and techniques for observing coastal ecosystems. In: Yang, X. (ed.), *Remote Sensing and Geospatial Technologies for Coastal Ecosystem Assessment and Management*. Berlin: Springer-Verlag.
- Klemas, V., 2009b. The role of remote sensing in predicting and determining coastal storm impacts. *Journal of Coastal Research*, 25, 1264–1275.
- Klemas, V., 2010. Tracking oil slicks and predicting their trajectories using remote sensors and models: case studies of the Sea Princess and Deepwater Horizon oil spills. *Journal of Coastal Research*, 25(5), 789–797.
- Klemas, V.; Dobson, J.E.; Ferguson, R.L., and Haddad, K.D., 1993. A coastal land cover classification system for the NOAA Coastwatch Change Analysis Project. *Journal of Coastal Research*, 9, 862–872.
- Klemas, V. and Philpot, W., 1981. Drift and dispersion studies of ocean-dumped waste using Landsat imagery and current drogues. *Photogrammetric Engineering and Remote Sensing*, 47, 533–542.
- Kohut, J.; Roarty, H.; Lichtenwalner, S.; Glenn, S.; Barrick, D.; Lipa, B., and Allen, A., 2008. Surface current and wave validation of a nested regional HF radar Network in the Mid-Atlantic Bight. In: *Current Measurement Technology, 2008. CMTc 2008. IEEE/OES 9th Working Conference*. pp. 203–207.
- Krabill, W.B.; Wright, C.W.; Swift, R.N.; Frederick, E.B.; Manizade, S.S.; Yungel, J.K.; Martin, C.F.; Sonntag, J.G.; Duffy, M.; Hulslander, W., and Brock, J.C., 2000. Airborne laser mapping of Assateague National Seashore Beach. *Photogrammetric Engineering and Remote Sensing*, 66, 65–71.
- Lathrop, R.G.; Cole, M.B., and Showalter, R.D., 2000. Quantifying the habitat structure and spatial pattern of New Jersey (U.S.A.) salt marshes under different management regimes. *Wetlands Ecology and Management*, 8, 163–172.
- Li, M.; Zhong, L.; Boicourt, W.C.; Zhang S., and Zhang, D., 2007. Hurricane-induced destratification and destratification in a partially-mixed estuary. *Journal of Marine Research*, 65, 169–192.
- Linker, L.C.; Stigall, G.E.; Chang, C.H., and Donigian, A.S., 1993. The Chesapeake Bay Watershed Model. In: *USEPA and Computer Sciences Corporation, Report CSC.MD1J.7/93*, pp. 1–9.
- Liu, G.; Strong, A.E.; Skirving, W., and Arzayus, L.F., 2005. Overview of NOAA coral reef watch program's near-real time satellite global coral bleaching monitoring activities. *Proceedings of the 10th International Coral Reef Symposium, Okinawa, Japan*, 1, 1783–1793.
- Lu, Z.; Kim, J.-W.; Lee, H.; Shum, C.K.; Duan, J.; Ibaraki, M.; Akyilmaz, O., and Read, C.-H., 2009. Helmand River Hydrologic Studies Using ALOS PALSAR InSAR and ENVISAT Altimetry. *Marine Geodesy*, 32, 320–333.
- Lunetta, R.S. and Elvidge, C.D., 1998. *Remote Sensing Change Detection: Environmental Monitoring Methods and Applications*. Chelsea, Michigan: Ann Arbor Press.
- Lyon, J.G. and McCarthy, J., 1995. *Wetland and Environmental Applications of GIS*. New York: Lewis Publishers.
- Maeder, J.; Narumalani, S.; Rundquist, D.; Perk, R.; Schalles, J.; Hutchins, K., and Keck, J., 2002. Classifying and mapping general coral-reef structure using Ikonos data. *Photogrammetric Engineering and Remote Sensing*, 68, 1297–1305.
- Marine Technology Reporter, 2010. Unmanned maritime vehicles. *Marine Technology Reporter*, March, 36–45.
- Martin, S., 2004. *An Introduction to Remote Sensing*. Cambridge, UK: Cambridge University Press.
- McClain, C.; Hooker, S.; Feldman, G., and Bontempi, P., 2006. Satellite data for ocean biology, biogeochemistry, and climate research. *AGU EOS Transactions*, 87, 337–343.
- Miller, J.L. and Goodberlet, M., 2004. Development and applications of STARRS: a next generation airborne salinity imager. *International Journal of Remote Sensing*, 25, 1319–1324.
- Miller, P.L.; Shutler, J.D.; Moore, G.F., and Groom, S.B., 2006. SeaWiFS discrimination of harmful algal bloom evolution. *International Journal of Remote Sensing*, 27, 2287–2301.
- Mishra, D.; Narumalani, S.; Rundquist, D., and Lawson, M., 2006. Benthic habitat mapping in tropical marine environments using QuickBird multispectral data. *Photogrammetric Engineering and Remote Sensing*, 72, 1037–1048.
- Morris, J.T.; Sundareshwar, P.V.; Nietch, C.T.; Kjerfve, B., and Cahoon, D.R., 2002. Responses of coastal wetlands to rising sea level. *Ecology*, 83, 2869–2877.
- Morton, R.A. and Miller, T.L., 2005. National assessment of shoreline change: Part 2. Historical shoreline change and associated coastal land loss along the U.S. Southeast Atlantic Coast. *US Geological Survey Open-File Report*, pp. 1401.
- Mumby, P.J. and Edwards, A.J., 2002. Mapping marine environments with IKONOS imagery: Enhanced spatial resolution can deliver greater thematic accuracy. *Remote Sensing of Environment*, 82, 248–257.
- NASA/GSFC (National Aeronautics and Space Administration/Goddard Space Flight Center), 2010. Hurricane Ike: storm surge flooding image of the Gulf Coast. NASA image courtesy Jeff Schmaltz, MODIS Rapid Response Team at NASA GSFC.
- NOAA (National Oceanic and Atmospheric Association), 1999. Trends in U.S. Coastal Regions, 1970–1998. Addendum to the Proceedings: Trends, and Future Challenges for U.S. National Ocean and Coastal Policy. NOAA, August.
- Odum, E.P., 1993. *Ecology and Our Endangered Life-Support Systems*, 2nd edition. Sunderland, Massachusetts: Sinauer Associates, Inc.
- Oliver, M.J.; Glenn, S.; Kohut, J.T.; Irwin, A.J.; Schofield, O.M.; Moline, M.A., and Bissett, W.P., 2004. Bioinformatic approaches for objective detection of water masses on continental shelves. *Journal of Geophysical Research*, 109, C07S04, doi:10.1029/2003JC002072.
- Orbimage, 2003. *OrbView-3 Satellite and Ground Systems Specifications*. Dulles, Virginia: Orbimage Inc.
- Paduan, J.D. and Graber, H.C., 1997. Introduction to high-frequency radar: reality and myth. *Oceanography*, 10, 36–39.
- Parkinson, C.L., 2003. Aqua: an Earth-observing satellite mission to examine water and other climate variables. *IEEE Transactions on Geoscience and Remote Sensing*, 41, 173–183.
- Philpot, W., 2007. Estimating atmospheric transmission and surface reflectance from a glint-contaminated spectral image. *IEEE Transactions on Geoscience and Remote Sensing*, 45, 448–457.
- Philpot, W.D.; Davis, C.O.; Bissett, P.; Mobley, C.D.; Kohler, D.D.; Lee, Z.; Snyder, W.A.; Steward, R.G.; Agrawal, Y.; Trowbridge, J.; Gould, R., and Arnone, R., 2004. Bottom characterization from hyperspectral image data. *Oceanography*, 17, 76–85.
- Pinet, P.R., 2009. *Invitation to Oceanography*, 5th edition. Sudbury, Massachusetts: Jones and Bartlett.
- Porter, D.E.; Field, D.W.; Klemas, V.V.; Jensen, J.R.; Malhotra, A.; Field, R.T.; and Walker, S.P., 2006. *RESAAP Final Report: NOAA/NERRS Remote Sensing Applications Assessment Project*. Columbia, South Carolina: University of South Carolina.
- Purkis, S.J.; Graham, N.A.J., and Riegl, B.M., 2008. Predictability of reef fish diversity and abundance using remote sensing data in Diego Garcia (Chagos Archipelago). *Coral Reefs*, 27, 167–178.
- Purkis, S.J.; Kenter, J.A.M.; Oikonomou, E.K., and Robinson, I.S., 2002. High-resolution ground verification, cluster analysis and optical model of reef substrate coverage on Landsat TM imagery (Red Sea, Egypt). *International Journal of Remote Sensing*, 23, 1677–1698.
- Ramsey, E. and Rangoonwala, A., 2005. Leaf optical property changes associated with the occurrence of *Spartina alterniflora* dieback in coastal Louisiana related to remote sensing mapping. *Photogrammetric Engineering and Remote Sensing*, 71, 299–311.
- Rasher, M.E. and Weaver, W., 1990. *Basic Photo Interpretation: A Comprehensive Approach to Interpretation of Vertical Aerial Photography for Natural Resource Applications*. Washington, DC: U.S. Department of Agriculture.
- Ritchie, J.R.; Zimba, P.V., and Everitt, J.H., 2003. Remote sensing techniques to assess water quality. *Photogrammetric Engineering and Remote Sensing*, 69, 695–704.
- Robinson, I.S., 1985. *Satellite Oceanography*. New York: John Wiley.

- Robinson, I.S., 2004. *Measuring the Oceans from Space: The Principles and Methods of Satellite Oceanography*. Berlin: Springer-Praxis.
- Sarabun, C., 1993. Observations of a Chesapeake Bay tidal front. *Estuaries*, 16, 68–73.
- Schmidt, K.S.; Skidmore, A.K.; Kloosterman, E.H.; Van Oosten, H.; Kumar, L., and Janssen, J.A.M., 2004. Mapping coastal vegetation using an expert system and hyperspectral imagery. *Photogrammetric Engineering and Remote Sensing*, 70, 703–716.
- Schofield, O.; Arnone, R.A.; Bissett, W.P.; Dickey, T.D.; Davis, C.O.; Finkel, Z.; Oliver, M., and Moline, M.A., 2004. Watercolors in the coastal zone: what can we see? *Oceanography*, June, 25–31.
- Schofield, O.; Kohut, J., and Glenn, S., 2008. Evolution of coastal observing networks. *Sea Technology*, 49, 31–36.
- Space Imaging, 2003. *IKONOS Imagery Products and Product Guide* (version 1.3). Denver, Colorado: Space Imaging LLC.
- Stockdon, H.F.; Sallenger, A.H.; List, J.H., and Holman, R.A., 2002. Estimation of shoreline position and change using airborne Lidar topographic data. *Journal of Coastal Research*, 18, 502–513.
- Stumpf, R.P., 2001. Applications of satellite ocean color sensors for monitoring and predicting harmful algal blooms. *Human and Ecological Risk Assessment*, 7(5), 1363–1368.
- Stumpf, R.P.; Culver, M.E.; Tester, P.A.; Kirkpatrick, G.J.; Pederson, B.; Tomlinson, M.C.; Truby, E.; Ransibrahmanakul, V.; Hughes, K., and Soracco, M., 2003. Use of satellite imagery and other data for monitoring *Karenia brevis* blooms in the Gulf of Mexico. *Harmful Algae*, 2, 147–160.
- Sydor, M., 2006. Use of hyperspectral remote sensing reflectance in extracting the spectral volume absorption coefficient for phytoplankton in coastal water: Remote sensing relationships for the inherent optical properties of coastal water. *Journal of Coastal Research*, 22, 587–594.
- Teague, C.C.; Vesecky, J.F., and Fernandez, D.M., 1997. HF radar instruments, past to present. *Oceanography*, 10, 40–44.
- Tester, P.A.; Stumpf, R.P.; Vukovich, F.M.; Fowler, P.K., and Turner, J.F., 1991. An expatriate red tide bloom: transport, distribution and persistence. *Limnology and Oceanography*, 36, 1053–1061.
- Thieler, E.R. and Danforth, W.W., 1994. Historical shoreline mapping: improving techniques and reducing positioning errors. *Journal of Coastal Research*, 10, 539–548.
- Tomlinson, M.C.; Stumpf, R.P.; Ransibrahmanakul, V.; Truby, E.W.; Kirkpatrick, G.J.; Pederson, B.A.; Vargo, G.A., and Heil, C.A., 2004. Evaluation of the use of SeaWiFS imagery for detecting *Karenia brevis* harmful algal blooms in the eastern Gulf of Mexico. *Remote Sensing of Environment*, 91, 293–303.
- Wang, Y., 2010. *Remote Sensing of Coastal Environments*. Boca Raton, Florida: CRC Press.
- Weatherbee, O.P., 2000. Application of satellite remote sensing for monitoring and management of coastal wetland health. In: Gutierrez, J. (ed.), *Improving the Management of Coastal Ecosystems through Management Analysis and Remote Sensing/GIS Applications*. University of Delaware Sea Grant Report, pp. 122–142.
- Wolter, P.T.; Johnston, C.A., and Niemi, G.J., 2005. Mapping submerged aquatic vegetation in the US Great Lakes using Quickbird satellite data. *International Journal of Remote Sensing*, 26, 5255–5274.
- Yan, X.-H.; Ho, C.; Zheng, Q., and Klemas, V., 1993. Using satellite IR in studies of the variabilities of the Western Pacific Warm Pool. *Science*, 262, 440–441.
- Yang, C.; Everitt, J.H.; Fletcher, R.S.; Jensen, J.R., and Mausel, P.W., 2009. Mapping black mangrove along the south Texas gulf coast using AISA+ hyperspectral imagery. *Photogrammetric Engineering and Remote Sensing*, 75, 425–436.
- Young, S.S. and Wang, C.Y., 2001. Land-cover change analysis of China using global-scale Pathfinder AVHRR Landcover (PAL) data, 1982–92. *International Journal of Remote Sensing*, 22, 1457–1477.
- Zhao, Z.; Klemas, V.; Zheng, Q.; Li, X., and Yan, X.H., 2004. Estimating parameters of a two-layer stratified ocean from polarity conversion of internal solitary waves observed in satellite SAR images. *Remote Sensing of Environment*, 94, 276–287.